CrystEngComm

Configurational and energetical study of the (100) and (110) surfaces of the MgAl2O4 spinel by means of quantum-mechanical and empirical techniques

Journal:	*CrystEngComm*
Manuscript ID:	CE-ART-06-2014-001217.R1
Article Type:	Paper
Date Submitted by the Author:	30-Jul-2014

Complete List of Authors:	Massaro, Francesco Roberto; Università degli Studi di Padova, Dipartimento di Geoscienze Bruno, Marco; Università degli Studi di Torino, Dipartimento di Scienze della Terra Nestola, Fabrizio; UNIPD, Geoscienze

Configurational and energetical study of the (100) and (110) surfaces of the $MgAl_2O_4$ spinel by means of quantum-mechanical and empirical techniques

Francesco Roberto MASSARO,[1]* Marco BRUNO,[2] Fabrizio NESTOLA[1]

[1]Dipartimento di Geoscienze – Università di Padova, via G. Gradenigo 6, I-35131 Padova, Italy

[2]Dipartimento di Scienze della Terra - Università di Torino, via Valperga Caluso 35, I-10125 Torino, Italy.

* *Corresponding author*
e-mail: francescoroberto.massaro@unipd.it
Tel.: +390116705140
Fax: +390116705128

Summary: This paper presents a detailed configurational analysis of the {100} and {110} crystallographic forms of the spinel *sensu stricto* ($MgAl_2O_4$). In order to collect as many structural and energetical data as possible about the most stable surface terminations, we have performed accurate calculations both at empirical and DFT level at 0K and in vacuum, by using a dedicated force field and the hybrid Hartree-Fock/Density Functional B3LYP Hamiltonian, respectively.

The configurational analysis performed in this work on $MgAl_2O_4$ will be useful for studying all of the minerals belonging to the family of the normal spinels (i.e, $MgCr_2O_4$). Indeed, the initial configurations found for the (100) and (110) faces of $MgAl_2O_4$ are the same for all of the normal spinels.

As concerns the (100) face, we found that the surface configuration with the lowest surface energy (1.596 J/m^2) is associated to the Mg-terminated one. Furthermore, we found an Al-O-terminated (100) configuration with a surface energy value (2.161 J/m^2) noteworthy lower than those previously calculated by other authors. This proves that for reaching an in-depth knowledge of a crystal surface, it is not sufficient to explore a limited number of terminations (configurations), but it is essential to perform a detailed crystallographic and configurational analysis of the face.

In the case of the (110) face and at variance with the (100), the most stable surface configuration (2.752 J/m^2) results to be an Al-O-terminated one.

Keywords: Spinel, surface energy, *ab initio* calculation, empirical calculation, configurational analysis, surface reconstruction.

1. Introduction

Spinel *sensu stricto* ($MgAl_2O_4$) is the commonest mineral in the spinel group. From the structural point of view,[1] spinels (space group *Fd3m*; a_0 = 8.08-8.54 Å; $\alpha = \beta = \gamma = 90°$) have general formula MN_2O_4 where M stands for the divalent cation (Mg, Fe, Zn, Mn, Ni) in four-fold coordination (A sites) and N is the trivalent cation (Al, Fe, Cr) with coordination number equal to six (B sites). Perpendicular to the triad axis, layers of oxygen ions alternate with layers of cations: the cation layers in which all the cations are six-fold coordinated alternate with layers in which all the cations are distributed among A and B sites in the ratio of 2:1. Two structural types occur, different in their cationic distribution: referring to the unit cell content, normal spinels (among which $MgAl_2O_4$) have 8 M^{2+} in A and 16 N^{3+} in B, while inverse spinels have 8 N^{3+} in A and 8 M^{2+} plus 8 N^{3+} in B. The spinel group may be subdivided into three series, according to whether N^{3+} is Al (spinel series), Fe (magnetite series) or Cr (chromite series).

Our interest for minerals in the spinel group (in particular magnesium chromite, $MgCr_2O_4$, secondly, $MgAl_2O_4$) is justified by the fact that they are typical diamond inclusions (DIs) in peridotitic rocks, along with orthopyroxene, diopsidic clinopyroxene, forsteritic olivine, piropic garnet and iron–nickel sulfides.[2] To determine whether these inclusions are *protogenetic* (they crystallize before the encapsulation by the host diamond) or *syngenetic* (inclusion and host diamond form at the same time) is fundamental for understanding the diamond formation processes. A substantial contribution to the syngenesis/protogenesis debate can come from the observation that some DIs occur in a specific orientation with respect to diamond; this can be considered as a proof of epitaxial relationship between DI and diamond, and hence of syngenesis.[3-8] A possible way to confirm this theory consists into determination of the interfacial free energy between DI and diamond. Indeed, this thermodynamical quantity allows to estimate the probability to have an epitaxial relationship between two phases during their mutual growth. But for calculating this quantity, a detailed knowledge of all the possible surface configurations of the phases involved is necessary. For this reason, in this work, we undertake a configurational study of the main crystal faces of $MgAl_2O_4$, whose bulk structure can be considered representative of all the normal spinels among which $MgCr_2O_4$ is included.

Furthermore, spinels are very interesting materials both from a fundamental and an applied point of view, being employed industrially in ceramics technology, materials science, and in heterogeneous catalysis.[9-11]

In all of these sectors the knowledge of the structure and energy of the crystal surfaces is fundamental to understand the chemical-physical processes involved. In particular, for the $MgAl_2O_4$

spinel, the main crystal faces to take into consideration are the (100), (110) and (111) ones; the most studied, both experimentally and theoretically, is the (100).

In order to determine the most stable surface structure (the one with the lowest surface energy) of the (100) face at 0K and in vacuum, previously published empirical and quantum-mechanical calculations were performed.[12-14] In all of these works, only stoichiometric surfaces (that is surface reconstructed to cancel out the dipole moment) were taken into account and a restricted number of (100) surface configurations were analyzed; unfortunately, in these papers there are not sufficient information and detailed figures that allow to understand and analyze the structure of the surface configurations. In detail, van del Laag et al.[12] have described only two surface configurations (Mg- and Al-terminated), whereas Fang et al.[13] individuated three surface configurations (Mg-, Al- and O-terminated), but they reported only the surface energy value of the Mg-terminated. Instead, Davies et al.[14] identified ten surface configurations (three Mg- and seven Al-O-terminated), giving a more complex and truthful description of the (100) surface structure of $MgAl_2O_4$ spinel. However, in all of these works, the Mg-terminated surface is always resulted to be that more stable,[12-14] with a surface energy value of the Al-O terminated higher than 3.0 J/m^2.[12]

Non stoichiometric surfaces were also investigated at theoretical level, since atomic force microscope (AFM) observations[15,16] revealed the presence of an unreconstructed (100) surface Al-O terminated. Otherwise stated, by using the same words of the authors, "*the (100) surface is terminated by an intact Al and O-terminated structure, which, in the thermodynamically stable configuration, exposes a significant number of surface Mg-Al antisite defects*". Furthermore, DFT calculations performed by the same authors[15,16] confirmed the higher stability of this Al-O terminated surface at different temperatures with respect to the Mg-terminated one, when the adsorption of H (with different configurations) is taken into account.

In this paper, we will deal with stoichiometric surfaces at 0K in vacuum and we will show that the number of surface configurations detected in the previous papers is not sufficient to give a correct description of the structural complexity of a crystal face of $MgAl_2O_4$ spinel. Furthermore, we will also show that the surface energy value of the more stable Al-O-terminated configuration found in the present work is noteworthy lower than those previously published.

The work has been structured as follows:

(i) Initially, a detailed configurational analysis of the (100) and (110) faces is performed, by using the working methodology recently developed by our research group and applied to the study of the (100), (110) and (112) faces of pyrope ($Mg_3Al_2Si_3O_{12}$).[17]

(ii) Then, we carried out empirical calculations about some selected (100) and (110) configurations (i.e., those preserving at least one element of symmetry perpendicular to the

face), adopting the force field developed by Smith et al.,[18] in order to determine their relaxed structures and surface energies. *Ab initio* quantum-mechanical calculations on the same configurations of the (100) face were simultaneously performed, by using a hybrid Hartree-Fock (HF)-DFT approach, which has never been applied before to the study of $MgAl_2O_4$ surfaces; the chosen functional is B3LYP,[19-21] which has already proved great accuracy in describing the surfaces of forsterite (Mg_2SiO_4)[22] and pyrope.[17]

(iii) Subsequently, the relaxed structures and surface energies of the more stable (100) configurations obtained with the two computational methodologies, are compared and discussed.

(iv) Finally, some general conclusions on the analysis and the way to face the study of the surface configurations of crystalline phases with complex structure and chemistry, are drawn. We want to give special attention to the importance of performing a detailed crystallographic analysis when the study of whatever crystal surface is faced.

2. Computational details

Optimizations of slab geometries and surface energy estimates were obtained by means of the GULP 4.0 and CRYSTAL09 simulation codes: the first was adopted for all the studied spinel configurations, the latter only for those belonging to the (100) surface. The GULP and CRYSTAL output files, listing the optimized fractional coordinates of the modelled configurations, are freely available at http://mabruno.weebly.com/download.

2.1. GULP

One set of calculations were performed by using the inter-atomic potential for $MgAl_2O_4$ developed by Smith et al.[18] and the GULP 4.0 simulation code[23] which, being based on force field methods, allows the calculation of structures and properties of minerals from a given set of empirical potentials. Geometry optimization is considered converged when the gradient tolerance and the function tolerance (*gtol* and *ftol* adimensional parameters in GULP) are smaller than 0.0001 and 0.00001, respectively.

The (100) and (110) surfaces of spinel were studied by using the 2D-slab model.[24] Slabs of varying thickness were generated by separating the optimized bulk structure (a = 8.0904 Å) along the plane of interest. The calculations were performed by considering the original (1×1) cells. The geometry optimization was performed by means of the Newton-Raphson method and by considering the slab subdivided into two regions: region 1, which contains both the surface and the underlying atomic layers that are allowed to relax, and region 2 which has the same number of

layers of the region 1, and contains the rest of the slab material where no relaxation with respect to the bulk crystal structure is assumed to occur.

The calculations were done by considering (100) slabs with thickness up to ~30 Å (equivalent to four d_{100}) and (110) slabs up to ~35 Å (equivalent to six d_{110}). They are sufficient to reproduce bulk-like properties at the centre of the slabs, to obtain a careful description of the surfaces and to reach convergence on the γ_{100} and γ_{110} values.

According to the standard two-regions strategy employed by GULP, the specific surface energy at T = 0K (γ, J/m^2) was evaluated from the energy of the surface block (U_s, region 1) and the energy of a portion of bulk crystal (U_b) containing the same number of atoms as the surface block. Both energies have been referred to A, the common surface area of the primitive unit cell:

$$\gamma = \frac{U_s - U_b}{A} \quad (1)$$

2.2. CRYSTAL

The crystal surfaces were simulated by using the 2D periodic slab model[24] and the *ab initio* CRYSTAL09 code.[25-27] The calculations (optimization of the fractional coordinates with fixed cell) were performed at the DFT (Density Functional Theory) level by means of the B3LYP Hamiltonian,[19-21] which already shown to provide accurate results for structural properties of forsterite[22] and pyrope.[17] Two different Gaussian basis sets reproducing the multi-electronic wave-function were adopted: (i) BS1, where aluminum, oxygen, and magnesium were described by (8*s*)-(511*sp*)-(1*d*), (8*s*)–(411*sp*)–(1*d*), and (8*s*)–(511*sp*)–(1*d*) contractions, respectively;[28,29] (ii) BS2, with aluminum, oxygen, and magnesium described by (73211*s*)-(5111*p*)-(1*d*), (6211*s*)-(411*p*)-(1*d*) and (73211*s*)-(511*p*)-(1*d*) contractions, respectively.[30] The quality of the BS1 basis set is lower than that of the BS2 basis set, as a consequence the accuracy of the calculations performed with BS1 is lower with respect to those carried out with BS2. Unfortunately, BS2 is time consuming from the computational point of view, therefore, first of all, we have performed all of the geometry optimizations of the *cut1* and *cut2* configurations of the (100) face by using BS1, then we have used BS2 only to optimize the two most stable surface configurations (*cut1* and *cut2*δ_{e3}, see the next paragraph) found with the BS1. Further computational details (e.g., thresholds controlling the accuracy of the calculations, integration grid, shrinking factor) are reported in the ESI.

All of the (100) slabs are charge neutral and retain the centre of inversion, in order to ensure that the dipole moment perpendicular to the slab is equal to zero.

The specific surface energy γ (erg/cm^2) at T = 0K was calculated with the relation:[24]

$$\gamma = \lim_{n\to\infty} E_s(n) = \lim_{n\to\infty} \frac{E(n)_{slab} - nE_{bulk}}{2A} \quad (2)$$

where $E(n)$ and E_{bulk} are the energy of a n-layer slab and of the bulk, respectively; A is the area of the primitive unit cell of the surface. $E_s(n)$ is thus the energy (per unit area) required for the formation of the surface from the bulk. When $n \rightarrow \infty$, $E_s(n)$ will converge to the surface energy per unit area (γ).

The thickness of the optimized slabs is ~13 Å (with 98 and 84 atoms for the *cut1* and *cut2* configurations, respectively). As in the case of the (100) face of pyrope,[17] for which a detailed analysis of the surface configurations was performed, a satisfactory convergence on structure is not reached and, as a consequence, thicker slabs should be considered. Unfortunately, the system studied is very demanding from a computational point of view, then we are not able to verify the criterion of convergence concerning the structure. Nevertheless, the slab thicknesses considered in this work are sufficient to obtain reliable surface energy values, which allow us to evaluate the most probable surface configuration. Indeed, previous *ab initio* calculations performed with the BS1 basis set, hybrid functional and computational parameters of this work on forsterite surfaces,[22] demonstrated that slab thickness of 14-15 Å are sufficient to reach convergence on surface energy values.

3. Configurational analysis of the spinel surfaces

In order to perform a geometry optimization, an initial crystal structure must be supplied to the program, i.e.: in our case as input in the CRYSTAL09 and GULP 4.0 codes. Then, each program will be able to find an optimized structure, according to its implemented computational strategy. As we previously showed for pyrope,[17] the study of each (*hkl*) face has to be conducted through the investigation of all the possible initial bulk-like surface configurations of the studied face.

The preliminary step consists of setting the phase structure as a stacked repetition of bulk slices meaningful from the structural and compositional point of view and to establish all the possible surface terminations obtained by cutting the bulk structure. Thus, it is possible to carry out a certain number of cuts placed at different levels of the bulk structure, for each {*hkl*} crystallographic form; each termination corresponds to a *cut* and has an its own surface cell. At the end of this phase, *slabs* built by an adequate number of atoms for the calculation, are generated by slicing the bulk structure according to the cut of interest.

In order to deal with the study of stoichiometric surfaces, each slab has to be made neutral and built by an integer number (n) of formula units, i.e.: $n\cdot(MgAl_2O_4)$. In order to achieve that, one

has the possibility to carve each slab, i.e.: removing the atoms from the outermost layers of the slab for obtaining a stoichiometric one, in different ways. Every single way corresponds to a different *surface configuration*. It is due to remember that the term *reconstruction* indicates the procedure of atoms removal to get a stoichiometric slab and that a *reconstruction slice* (RS, as defined in [17]) is a slice of variable thickness which is composed by the minimum number of outermost layers involved in the surface reconstruction; atoms having the same z-coordinate (according to the perpendicular to the plane of interest) in a not optimized slab, are considered to form a *layer*.

Summarizing, each {*hkl*} crystallographic form can have more cuts and each cut can have different surface configurations.

In the following paragraphs, the number and type of initial surface configurations of the {100} and {110} forms of spinel are determined. It is necessary to point out that:

(i) the slabs were cut starting from the optimized bulk structures: $\alpha = \beta = \gamma = 90°$ and $a_0 = 8.0904$ Å with the GULP code, and $a_0 = 8.1188$ Å (BS1) and $a_0 = 8.1547$ Å (BS2) with the CRYSTAL code;

(ii) unlike our methodological work on pyrope,[17] in which we imposed the constraint not to break the strong bonds in the Si tetrahedra, here the oxygen elimination does not follow any kind of restriction.

3.1 {100} form

Projecting along the <100>, we can imagine the spinel structure as a stacking of d_{800} slices of two sorts: one containing MgO_4 tetrahedra and the other made up by AlO_6 octahedra. It ensues that one can realize two cuts, namely *cut1* and *cut2*.

By analyzing the (100) slab structure, a square surface cell can be identified having surface vectors belonging to the <100> directions equal to 8.0904 Å and 8.1188-8.1547 Å for the GULP and the CRYSTAL BS1 and BS2 optimizations, respectively, and $\gamma = 90°$. For what concerns the symmetry elements, each cell shows four orders of *m* planes orthogonal two by two among themselves (oriented along the cell diagonals) and two orders of equivalent two-fold axes (eight in all) perpendicular to the face.

As concerns *cut1*, the RS is formed by one layer of Mg whose centres of mass coincide with some of the two-fold axes (left of Figure 1). For obtaining a stoichiometric slab, one Mg cation every two has to be removed from each cell, thus preserving two families of orthogonal *m* planes and one of two-fold axes. As the two-fold axis coincide with the Mg ions, only one independent surface configuration originates, in the following named *cut1* (see the upper-left drawing of Figure 2).

The *cut2* has a higher atomic density with respect to the *cut1*. The RS is composed by three layers: the uppermost containing the oxygens bonded to Mg ions (O1 from now on), the intermediate made up only by aluminiums, and a lower one built by the oxygens exclusively linked to the Al cations (O2 from now on). The stoichiometric rule implies a 50% reconstruction, that is the elimination of two Al every four and four O anions every eight.

FIGURE 1

In order to better organize the reconstruction procedure for the *cut2*, we identified five general cases that arise from the number of O1 and O2 involved.

a) The α reconstruction is the only one that preserves the entirety of the MgO_4 tetrahedra, thus all the resulting configurations are lacking of O2. Matching the only configuration coming from the O2 elimination and the three (*1*, *2* and *3* from now on) deriving from the arrangement of Al, three possible surface configurations come out in all. In detail, $cut2\alpha_1$ and $cut2\alpha_3$ are configurations with higher symmetry, keeping two orders of orthogonal *m* planes and one family of two-fold axes each, while $cut2\alpha_2$ only preserves two orders of parallel *m* planes.

b) In the β reconstructions no MgO_4 tetrahedron survives, thus all the resulting configurations are lacking of O1. Among the three possible surface configurations, $cut2\beta_1$ and $cut2\beta_3$ preserve two orders of orthogonal *m* planes and one of two-fold axes each, while $cut2\beta_2$ only keeps two families of parallel *m* planes.

c) The γ reconstructions are realized eliminating one O1 and three O2 from the *cut2* slab. Matching the four ways (named *a*, *b*, *c* and *d*) to remove the oxygens and the three to eliminate the Al, twelve surface configurations originate. In every case the symmetry of the face falls down.

d) The δ reconstructions are realized taking away two O1 and two O2 from the *cut2* slab. Matching the seven ways (named with the letters from *a* to *g*) to remove the oxygens and the three to eliminate the Al, twenty-one surface configurations originate. Among the possible surface configurations, only $cut2\delta_{b3,c2,d1,e1,e3,f1}$ and $_{f3}$ preserve one family of *m* planes, while $cut2\delta_{a1}$ and $cut2\delta_{g1}$ keep one family of two-fold axes.

e) The ε reconstructions are realized eliminating three O1 and one O2 from the *cut2* slab. As in the γ cases, matching the four ways to cancel the oxygens and the three to eliminate the Al, twelve surface configurations with no symmetry arise.

FIGURE 2

This work takes only into account the surface configurations respecting the symmetry of the face, as we previously demonstrated[31-35] that such surfaces are associated to lower surface energy values, thus they have a higher chance to exist at the equilibrium or in growth. Therefore, the most stable surface termination is to research into the sixteen initial configurations (Figure 2) among the fifty-two identified (see Figure S1 and S2 in the ESI for details about all the configurations). In a next paragraph, the surface energy values and optimized structures of these configurations obtained at *ab initio* and empirical levels will be discussed.

3.2 {110} form

Projecting along one of the <110> directions, one can imagine the spinel structure as a stacking of d_{440} slices made up by MgO_4 tetrahedra and AlO_6 octahedra, and d_{440} slices of only AlO_6 octahedra. As in the (100) case, it is possible to perform two sorts of cuts, namely *cut1* and *cut2*.

The (110) slab structure shows a rectangular 2D surface cell limited by <110> (equal to 11.4415 Å for the GULP optimizations) and <100> vectors and $\gamma = 90°$. The (110) surface cell has two orders of parallel *m* planes oriented along the shortest dimension and two orders of equivalent two-fold axes (four plus four) perpendicular to the face.

FIGURE 3

The *cut1* RS cell is formed by a unique layer made by four Mg, eight O1 and four Al whose centres of mass coincide with half of the two-fold axes (left of Figure 3). In order to obtain a stoichiometric slab, one Mg cation every four has to be deleted from each cell, thus preserving one family of *m* planes, from which only one independent surface configuration originates, in the following named *cut1* (see the upper-left drawing of Figure 4).

The *cut2* has a slightly lower atomic density with respect to the *cut1*. Starting from the highest z-coordinates, the RS is composed by an uppermost layer containing four O1, an intermediate one made by four Al and a lower one built by four O2. The stoichiometric constraint implies a 50% reconstruction, that is the elimination of two Al every four and four O anions every eight.

As for the (100) face, we identified five general cases that arise from the number of O1 and O2 removed during the reconstruction.

a) The α configurations are obtained removing all the O2, thus preserving the entirety of the MgO_4 tetrahedra. Matching the only configuration coming from the O2 elimination and the three coming out from the arrangement of Al, three possible surface configurations take place. In detail, the $cut2\alpha_1$ configuration keeps the *m* planes, while $cut2\alpha_2$ and $cut2\alpha_3$ only preserves one order of two-fold axes.
b) In the β reconstructions all the O1 are cancelled from the RS. Among the three possible surface configurations, $cut2\beta_1$ keeps the *m* planes, while $cut2\beta_2$ and $cut2\beta_3$ preserves one family of two-fold axes.
c) The γ configurations are built removing one O1 and three O2 from the *cut2* slab. Among the consequent twelve surface configurations, obtained matching the four ways to remove the oxygens and the three to eliminate the Al, only two ($cut2\gamma_{c1}$ and $cut2\gamma_{d1}$) keep one family of *m* planes.
d) The δ reconstructions are realized removing two every four oxygens of both the type 1 and 2 from the *cut2* slab. Matching the eight ways (named with the letters from *a* to *h*) to remove the oxygens and the three to eliminate the Al, twenty-four surface configurations originate. Among these, only $cut2\delta_{a2,c2,g3}$ and $_{h3}$ show somewhat symmetry, all preserving one family of two-fold axes.
e) The ε reconstructions are realized taking away three O1 and one O2 from the *cut2* RS. As in the γ cases, combining the four ways to remove the oxygens and the three to eliminate the Al, twelve surface configurations symmetry arise, of which $cut2\varepsilon_{a1}$ and $cut2\varepsilon_{c1}$ keep one family of *m* planes.

FIGURE 4

One has to look for the most stable (110) surface termination into the symmetrical fifteen initial configurations (Figure 4) among the fifty-five identified on the whole (see Figure S3 and S4 in the ESI). The study of these configurations was carried out only at empirical level.

4. Results and discussion.

In this paragraph, the energies and structures of the optimized surface configurations belonging to the {100} and {110} crystallographic forms of the Mg-spinel will be discussed. Table 1 lists the surface energies at 0K (γ) of the sixteen symmetrical configurations of the {100}. The calculations were performed at empirical and *ab initio* level; in order to be more accurate, we decided in the latter case to use the BS2 (see Computational Details) for the lowest energy cuts resulting from the

BS1 calculations. The same table shows results about the fifteen configurations referring to the {110}, studied exclusively by means of empirical force fields.

Table 1. Surface energies at 0K of all the symmetrical initial configurations of the spinel {100} and {110} calculated, the first both at empirical and quantum-mechanical level, while the second only at empirical level. The dashed boxes refer to calculations that have not reached the convergence. The $\Delta\gamma$ (%) = $[(\gamma_{FF} - \gamma_{BS1})/ \gamma_{BS1}]\times100$ for each configuration is reported as well.

cut	**{100} surface energies** [J/m^2]			**Δγ** [%]	*cut*	**{110} surface energies** [J/m^2]
	FF	**BS1**	**BS2**			**FF**
1	2.315	1.924	1.596	+20.3	*1*	3.084
$2\alpha_1$	3.573	3.362		+6.3	$2\alpha_1$	3.522
$2\alpha_2$	4.026	3.390		+18.8	$2\alpha_2$	3.341
$2\alpha_3$	6.160	-		-	$2\alpha_3$	3.340
$2\beta_1$	3.757	5.755		-34.7	$2\beta_1$	3.634
$2\beta_2$	3.645	3.465		+5.2	$2\beta_2$	2.752
$2\beta_3$	4.281	3.251		+31.7	$2\beta_3$	2.810
$2\delta_{a1}$	3.357	2.905		+15.6	$2\gamma_{c1}$	3.677
$2\delta_{b3}$	4.279	-		-	$2\gamma_{d1}$	3.813
$2\delta_{c2}$	3.810	3.506		+8.7	$2\delta_{a2}$	2.808
$2\delta_{d1}$	3.183	2.783		+14.4	$2\delta_{c2}$	2.752
$2\delta_{e1}$	4.334	3.076		+40.9	$2\delta_{g3}$	2.807
$2\delta_{e3}$	2.766	2.603	2.161	+6.3	$2\delta_{h3}$	2.753
$2\delta_{f1}$	4.261	-		-	$2\varepsilon_{a1}$	3.382
$2\delta_{f3}$	2.741	2.626		+4.4	$2\varepsilon_{c1}$	3.509
$2\delta_{g1}$	4.744	5.896		-19.5		

4.1 {100} form

The configuration with the lowest surface energy results to be by far the *cut1*. This happens regardless the calculus technique, even if the BS1 value is ~20% lower than the FF one. A more accurate estimation by means of the BS2 beats down this energy by an additional 17% to 1.596 J/m^2. The surface profiles of *cut1* resulting from the three simulation methods are showed in the relaxed state in the upper part of Figure 5. Despite the energy differences, the three structures appear to be almost identical apart from the position of the uppermost magnesium ion that clearly lowers to flatten down on the surface in the quantum-mechanical simulations.

The *cut2* configuration with the lowest energy is the *cut2*δ_{e3}. For this surface the BS1 value is more near (~6% lower) respect to the FF one, while the estimation adopting the BS2 brings again to a further energy decrease by 17% to 2.161 J/m^2. As the lower part of Figure 5 proves, it is not possible to appreciate by eyes differences among the geometries respective to the profile optimized by the different techniques.

Some further considerations about the γ values obtained using the FF and the BS1 methods can be done. As expected, the BS1 values are generally lower than the FF ones, the gap varying from ~4% in the $2\delta_{f3}$ case to ~41% in the $2\delta_{e1}$ case. Nevertheless, the BS1 optimization leads to higher energy values respect to the FF calculations in the case of the $2\beta_1$ and $2\delta_{g1}$ configurations for which we have registered an increase by ~35 and ~20%, respectively.

A careful examination of the structures relaxed by using the BS1 let one deduce that the twelve (100) configurations whose computation reaches the convergence, are actually less if taking into account the geometrical affinities. In confirmation of this, the surface cuts that are similar from a geometrical point of view have also very similar surface energies, excluding the $cut2\delta_{d1}$ and δ_{e1} configurations, since they show a different alignment degree of the uppermost Al and O along the equivalent <100> directions. The couples of surfaces of a kind ordered by decreasing of stability are $2\delta_{e3}$ and $2\delta_{f3}$, $2\delta_{d1}$ and $2\delta_{e1}$, $2\alpha_1$ and $2\alpha_2$. After the optimization procedure, the twelve initial surface configurations have became nine, among which we are able to distinguish: (i) the absolute minimum of the potential energy surface corresponding to the optimized structure of *cut1*; (ii) eight local minima corresponding to the others optimized structures. The percentage variation of the surface energy of the *i*-th configuration with respect to the most stable one results to be ~35-36% for the $cut2\delta_{e3}$-δ_{f3}, ~45-60% for the $cut2\delta_{d1}$-δ_{e1}, ~51% for the $cut2\delta_{a1}$, ~69% for the $cut2\beta_3$, ~75-76% for the $cut2\alpha_1$-α_2, ~80% for the $cut2\beta_2$, ~82% for the $cut2\delta_{c2}$, ~199% for the $cut2\beta_1$ and ~206% for the $cut2\delta_{g1}$. Interestingly, the smallest percentage difference is big enough to suggest that the probability to have a (100) surface with the *cut1* configuration is very high.

FIGURE 5

In the following part, some considerations about the modifications of the Cation-Oxygen bond lengths and of the Oxygen-Cation-Oxygen angles are discussed. After the reconstruction, the {100} surface cations loose their original coordination, i.e.: the bulk coordination. In detail, the 4-fold coordination of the bulk Mg reduces to 2 and 3 in the *cut1* and *cut2* RS cells, respectively, while the 6-fold coordination of the bulk Al changes to 5 in the *cut1* and 4 in the *cut2*. As a consequence, the initial 6 O-Mg-O angles reduce to 1 and 3 in the *cut1* and *cut2* RS cells, respectively, while the 15 O-Al-O angles become 10 in the *cut1* and 6 in the *cut2*.

Table 2 reports the values for the Mg-O and Al-O bond distances for the optimized bulk and the two kind of cuts according to which it is possible to realize the lowest energy {100} surfaces (cuts *1* and $2\delta_{e3}$). Two statistical indices are adopted:

- the first is useful to summarize the effect of atomic relaxation. It is the average Cation-O bond distance per polyhedron, <Cation-O> [Å], thus one can appreciate the percentage difference between these lengths in the uppermost atoms of the RS and those in the bulk;
- the second gives a comparison among the three calculation procedures in relation to the one considered the most reliable, i.e.: the quantum-mechanical calculus by means of BS2. It is the percentage difference Δ [%], between the bond lengths calculated by whatever method respect to those calculated by means of the BS2.

The average values calculated for the Mg-O and Al-O bulk distances are 1.9375, 1.9466 and 1.9565 Å, and 1.9213, 1.9269 and 1.9347 Å for the FF, BS1 and BS2, respectively. The BS2 technique leads to bulk bonds somewhat larger than those coming from the other methods. The same bonds reduce in the optimized RS cell by ~0.5% in the Mg-O case (both for the *cut1* and the *cut2*), while the Al-O bonds shorten by ~1.6 and ~7.3% in the *cut1* and in the *cut2*, respectively. The same distances computed with the FF and BS1 techniques do not move away from this general trend apart from the *cut1* Mg-O bond calculated by the GULP-FF method for which we have registered a reduction by ~8.3% respect to the bulk value. Comparing the three ways of calculating through the Δ index, one can notice that, as expected, the quantum-mechanical ways are much similar between them. However, the empirical way is not so far for all the bulk or *cut1/2* <Cation-O> distances (the Δ being not much higher than ~1%), except for the above mentioned Mg-O bond in the *cut1* for which the Δ index undergoes a reduction by ~9%.

From the evaluation of the Cation-O distances one can deduce that the Mg and Al surface cations, which loose their original coordination (i.e.: the bulk coordination), result to be more attracted by the remaining oxygens. The same thing does not happen in the case of the *cut2* uppermost Mg studied with the BS1, for which a very weak rise (0.06%) of the Mg-O bond length is observed.

Table 2. Optimized Mg-O and Al-O bond distances [Å] of bulk-spinel and of its (100) surface according to the two lowest energy terminations at 0 K, each for the two kinds of cut. The listed data refer to each empirical potential and basis set adopted for the calculation. Surface data are reported for the symmetry independent polyhedra included in the reconstruction slice. <Cation-O> [Å] is the average bond length per polyhedron and Δ [%] is the difference between the <Cation-O> distances calculated by whatever method and those by means of the BS2. The relative % difference of <Cation-O> in the surface cut respect to the bulk, and the multiplicity m of the bulk bonds are reported as well.

	FORCE FIELD				**BASIS SET 1**				**BASIS SET 2**			
bond	m	bulk	(100)		m	bulk	(100)		m	bulk	(100)	
			cut1	*cut2*			*cut1*	*cut2*			*cut1*	*cut2*
Mg-O	4	1.9375	1.7885	1.8975	4	1.9466	1.9441	1.9244	4	1.9565	1.9467	1.9171
			1.7885	1.9343			1.9441	1.9589			1.9470	1.9598
				1.9447				1.9603				1.9613

<Mg–O>	1.9375	1.7885	1.9255	1.9466	1.9441	1.9478	1.9565	1.9469	1.9460
		-8.33%	-0.62%		-0.13%	+0.06%		-0.50%	-0.54%
Δ	-0.98%	-8.85%	-1.07%	-0.51%	-0.14%	+0.09%	0.00%	0.00%	0.00%
Al-O	6 1.9213	1.8431	1.7134	6 1.9269	1.8167	1.6902	6 1.9347	1.8255	1.7044
		1.8510	1.7843		1.8516	1.7580		1.8657	1.7685
		1.8763	1.8487		1.8781	1.8310		1.8832	1.8488
		1.8836	1.8694		1.9477	1.8809		1.9513	1.8880
		1.9731			1.9771			1.9962	
<Al–O>	1.9213	1.8854	1.8040	1.9269	1.8942	1.7900	1.9347	1.9044	1.8024
		-1.90%	-6.51%		-1.72%	-7.65%		-1.59%	-7.34%
Δ	-0.70%	-1.00%	+0.09%	-0.40%	-0.53%	-0.69%	0.00%	0.00%	0.00%

Table 3 lists the O-Mg-O and O-Al-O bond angles for the bulk and the cuts *1* and $2\delta_{e3}$. Again, two statistical indices are adopted to evaluate the effect of geometry optimization (i.e.: the average O-Cation-O bond angle per polyhedron, <O-Cation-O> [°]) and to compare the calculation methods (i.e.: the difference between the bond angles calculated by whatever method respect to those calculated by means of the BS2, Δ [%]). The average values computed for the O-Mg-O (109.471°) and O-Al-O (108.000°) bulk angles are identical for the FF, BS1 and BS2 methods. The most significant angular variations from the bulk values after relaxation are observed in the O-Mg-O case; again, the *cut1* O-Mg-O angle calculated by the GULP-FF method moves a lot away, increasing by ~20% respect to the bulk value and by ~19% respect to the BS2 value. On the other hand, regardless the computational method, the O-Al-O angles follow the same trend: they reduce by ~0.5% in the *cut1* and enlarge by ~1% in the *cut2*.

Table 3. Optimized O-Mg-O and O-Al-O bond distances [Å] of bulk-spinel and of its (100) surface according to the two lowest energy terminations at 0 K, each for the two kinds of cut. The listed data refer to each empirical potential and basis set adopted for the calculation. Surface data are reported for the symmetry independent polyhedra included in the reconstruction slice. <O-Cation-O> [°] are the average bond angles per polyhedron and Δ [%] is the difference between the <O-Cation-O> angles calculated by whatever method and those by means of the BS2. The relative % difference of <O-Cation-O> in the surface cut respect to the bulk, and the multiplicity m of the bulk bonds are reported as well.

	FORCE FIELD				**BASIS SET 1**				**BASIS SET 2**			
angle	m	bulk	(100)		m	bulk	(100)		m	bulk	(100)	
			cut1	*cut2*			*cut1*	*cut2*			*cut1*	*cut2*
O-Mg-O	6	109.471	136.741	109.729	6	109.471	111.443	109.083	6	109.472	111.318	109.490
				117.088				114.626				116.369
				117.088				115.127				117.015
<O–Mg–O>		109.471	136.741	114.635		109.471	111.443	112.945		109.472	111.318	114.291
			+19.94%	+4.50%			+1.77%	+3.08%			+1.66%	+4.22%
Δ		0.00%	+18.59%	+0.30%		0.00%	+0.11%	-1.19%		0.00%	0.00%	0.00%

O-Al-O	6	83.425	77.432	86.948	6	84.755	79.655	88.138	6	83.288	79.650	87.286
	6	96.575	82.736	91.516	6	95.225	81.589	93.557	6	96.712	81.887	93.140
	3	180.000	86.189	93.940	3	180.000	87.032	94.615	3	180.000	86.660	94.290
			86.280	107.288			87.451	110.033			86.966	108.710
			93.744	112.218			93.952	113.719			93.737	112.593
			100.617	161.389			101.284	154.871			101.362	158.046
			104.512				103.372				103.024	
			104.934				104.555				104.242	
			168.510				167.400				168.010	
			168.756				168.830				169.538	
<O–Al–O>		108.000	107.371	108.883		108.000	107.512	109.155		108.000	107.508	109.011
			-0.59%	+0.81%			-0.45%	+1.06%			-0.46%	+0.93%
Δ		0.00%	-0.13%	-0.12%		0.00%	0.00%	+0.13%		0.00%	0.00%	0.00%

4.2 {110} form

The configurations with the lowest surface energy computed by the GULP-FF method result to be *cut2*β_2 and $2\delta_{c2}$, both having a γ value equal to 2.752 J/m^2. As in the {100} case, there is only a configuration referring to the *cut1*, whose γ value is 3.084 J/m^2. The above mentioned {110} optimized surface profiles (in detail the *cut1* and *cut2*β_2) are showed in the relaxed state in Figure 6. The effects of relaxation are more clear in the stable *cut2* case, for which it is possible to observe the translation of a few Mg ions and of some oxygens bonded to the Al ions near the surface. After the reconstruction, both the 4-fold coordination of the bulk Mg and the 6-fold coordination of the bulk Al reduce to 3 in each cut RS cell. It ensues that the initial 6 O-Mg-O angles reduce to 3, while the 15 O-Al-O angles become 6 in every configuration.

Table 4 lists the bond lengths and angles regarding the surface Mg and Al ions belonging to the cuts *1* and $2\beta_2$. One more time, two statistical indices are adopted to evaluate the effect of geometry optimization, i.e.: the average Cation-O bond distance, <Cation-O> [Å] and the average O-Cation-O bond angle, <O-Cation-O> [°]. Looking at the table, it is possible to confirm a general trend already reported for the {100} form: surface relaxation leads the Cation-O bonds to become smaller, whereas the O-Cation-O tend to rise except a few O-Al-O angles. The most significant distortions from the bulk concern the Al-O bonds (smaller by ~9% in the *cut1* and by ~6% in the *cut2*) and the O-Mg-O angles (larger by ~5% in the *cut1* and by ~4% in the *cut2*).

Table 4. Optimized Mg and Al bonds and angles respect to oxygen atoms of the spinel (110) surface according to the two lowest energy terminations at 0 K calculated for the two kinds of cut. The listed data refer to calculation based on empirical potentials. Surface data are reported for the symmetry independent polyhedra included in the reconstruction slice. <Cation-O> [Å] is the average bond length per polyhedron; the relative % difference of <Cation-O> and the multiplicity m of the bulk bonds are reported as well.

bond/angle	m	bulk	(110)		bond/angle	m	bulk	(110)	
			cut1	*cut2*				*cut1*	*cut2*
Mg-O	4	1.9375	1.8454	1.8735	Al-O	6	1.9213	1.7295	1.6824
			1.8658	1.8968				1.7607	1.8450
			1.8863	1.9633				1.7802	1.8518
								1.8018	1.8866
<Mg–O>		1.9375	1.8556	1.9112	<Al–O>		1.9213	1.7680	1.8164
			-4.41%	-1.38%				-8.67%	-5.77%
O-Mg-O	6	109.471	108.579	103.622	O-Al-O	6	83.425	90.562	83.556
			116.260	114.845		6	96.575	93.520	88.248
			119.875	122.734		3	180.000	102.543	91.956
								104.575	96.898
								110.307	110.671
								150.569	161.000
<O–Mg–O>		109.471	114.875	113.734	<O–Al–O>		108.000	108.679	105.390
			+4.70%	+3.75%				+0.62%	-2.48%

FIGURE 6

6. Conclusions

In this paper, we have applied the working methodology recently developed by our research group[17] to find all the possible surface configurations of the (100) and (110) faces of $MgAl_2O_4$ normal spinel. Then, we have performed empirical calculations at 0K, by adopting the force field developed by Smith et al.,[18] in order to determine the relaxed structures and surface energies of the (100) and (110) configurations. Finally, we have performed an accurate *ab initio* study of the structures and surface energies at 0K of the (100) configurations, by using for the first time, at the best of our knowledge, the hybrid Hartree-Fock/Density Functional B3LYP Hamiltonian and a localized all-electron Gaussian-type basis set.

In the following, our results and considerations are summarized:

(i) 52 initial surface configurations were identified for the (100) face, but only 16 preserve some elements of symmetries (i.e., a diad axis and/or a mirror plane perpendicular to the face). These symmetrical configurations were used as guess input geometries into the GULP and CRYSTAL programs for performing *empirical* and *ab initio* calculations and determining in this way the equilibrium structure and surface energy of the most stable surface termination of the (100) face. After the minimization procedure, we found that the surface configuration with the lowest surface energy (1.596(BS2)-2.315(FF) J/m^2) is associated to the *cut1* (i.e, the Mg-terminated surface). This finding is in agreement with the previous ones.[12-14] In detail: (i) van

der Laag et al.[12] reports a surface energy value, obtained at *ab initio* level, of 1.61 J/m^2, very close to our estimate by using BS2; (ii) values of 2.27-2.28 J/m^2, also in this case very similar to our estimate, were calculated at empirical level by Fang et al.[13] and Davies et al.[14]

(ii) We found an Al-O-terminated (100) configuration (*cut2*δ_{e3}) with a surface energy value (2.161(BS2)-2.766(FF) J/m^2) noteworthy lower than those previously calculated by van der Laag et al.[12] and Davies et al.,[14] which obtained 3.10 and 3.25 J/m^2, respectively. This proves that for reaching an in-depth knowledge of a crystal surface, it is not sufficient to explore a limited number of terminations (configurations), but it is essential to perform a detailed crystallographic and configurational analysis of the face. Indeed, Laag et al.[12] and Davies et al.[14] did not find the most stable Al-O-terminated surface configuration, because they did not perform a complete configurational study of the (100) face, but they limited their analysis to a restricted group of configurations.

Always concerning the configurational analysis, it is advisable to treat the crystal surface as a *crystallographic entity* and not exclusively as a chemical system lacking of whatever symmetry. As a matter of fact, when a crystal face is studied, it is fundamental to specify the symmetry elements preserved, if any, in the different surface configurations, as well as the cell parameters of the 2D cell considered. In this way a complete description of the surface is given and the reproducibility of the data is guaranteed.

(iii) The force field employed in this work[18] has been able to identify the two most stable surface configurations of the (100) face (*cut1* and *cut2*δ_{e3}). The optimized surface structures resulting from the empirical calculations are very similar to those obtained at *quantum-mechanical* level, whereas a high discrepancy exists between empirical and *ab initio* surface energy values. This suggests that in this case the employment of a force field can be useful to individuate, among all those possible, the surface configuration with the lowest surface energy, but only *ab initio* calculations can give reliable values of this quantity.

(iv) We have performed empirical calculations for individuating the most stable surface configuration at 0K of the (110) face, which is associated to *cut2*β_2, with a surface energy of 2.752 J/m^2. This value is in good agreement with those reported and calculated at empirical level by Fang et al.[13] and Davies et al.:[14] 2.85 and 2.90 J/m^2, respectively. However, according to what reported at point (iii), to have reliable estimates of the surface energy it is necessary to perform *ab initio* calculations.

(v) At 0K, in the vacuum, among all of the surface configurations analysed, the most stable one results to be the Mg-terminated (*cut1*) for the (100) face and the Al-O-terminated (*cut2*β_2) for the (110). It is important to stress here that the stability order of the surface configurations

obtained in this work can be completely modified when a thermodynamic equilibrium with an oxygen-rich environment (ambient conditions) is considered.[36] Despite this, the importance of our work does not diminish, because only performing the thermodynamic analysis to all of the surface configurations it is possible to evaluate the most probable surface termination at ambient conditions.

(vi) The configurational analysis performed in this work on $MgAl_2O_4$ will be useful for all of the people working on minerals belonging to the family of the normal spinels (i.e, $MgCr_2O_4$). Indeed, the initial configurations found for the (100) and (110) faces of $MgAl_2O_4$ are the same for all of the normal spinels. Obviously, empirical and/or *ab initio* calculations must be performed to study how the chemistry (e.g., Cr in place of Al) affects the stability of the different surface configurations.

(vii) In this work the importance of the basis set used for performing *ab initio* calculations on the surfaces is put in evidence. Indeed, the estimates of the (100) surface energy performed by adopting BS2 are 1.596 (*cut1*) and 2.161 ($cut2\delta_{e3}$) J/m^2, which are lower by 17% then those obtained with BS1, 1.924 (*cut1*) and 2.603 ($cut2\delta_{e3}$) J/m^2. Moreover, it is highly probable that the surface energy values obtained with BS2 could be further reduced when the BSSE (basis set superposition error) is also taken into account. However, before to draw conclusions about this argument, a detailed and systematic computational study discussing the effect of several basis sets, Hamiltonians and BSSE on the (100) surface of $MgAl_2O_4$ must be done. At the time being, we can only state that the basis set BS1 is not suitable to compute accurate values of the surface energy.

(viii) We performed empirical and *ab initio* calculations by considering the minimum surface cell ((100)-1x1 and (110)-1x1) that allows to perform the reconstruction to obtain a stoichiometric slab. Variable surface cells (i.e., (100)-2x1, (100)-2x2) should be also considered, to increase the degree of freedom of the structure and obtain the configuration with the lowest surface energy. However, we performed an empirical calculation by considering a (100)-2x1 cell for *cut1*, without observing a significant energy variation respect to the (100)-1x1 cell. Therefore, we believe that our results are not affected by this restriction.

(ix) It is important to point out that for a correct study of the stability of a surface, the effect of the temperature should also be taken into account. We only considered the surface energy at 0K, but it is important to know how this quantity changes with temperature by considering the entropic contribution due to the vibrational motion of atoms at its surface (vibrational entropy). As recently demonstrated for NaCl and LiF,[33,35,37] the effect of the temperature on the surface energy values is not negligible, observing for the (100) face of these phases a

surface energy decreases of ~10-15% by increasing the temperature from T = 0 to T = 300 K. Despite that, we believe that for the different (100) and (110) surface configurations the decrease of the surface energy due to the temperature is not so different to strongly affect our findings at 0K.

Electronic Supplementary Information (ESI) Available. Drawings of all the fifty-two and fifty-five possible surface configurations of the spinel {100} and {110} crystallographic forms, respectively. Computational details of the quantum-mechanical calculations performed on the (100) face.

Acknowledgements

The study was financially supported by ERC 7th Framework Programme "Ideas" Specific Programme, project INDIMEDEA to FN (grant agreement n° 307322). Thanks are due to two anonymous reviewers for their careful reading of the manuscript and their fundamental observations on our work.

References

1 W.A. Deer, R.A. Howie, J. Zussman, *An Introduction to the Rock-Forming Minerals*; Longman Ed.: Burnt Mill, Harlow, Essex, England, 1992; 2nd edition, p.558.

2 F. Nestola, M. Merli, P. Nimis, M. Parisatto, M. Kopylova, A. De Stefano, M. Longo, L. Ziberna, M. Manghnani, *European Journal of Mineralogy*, 2012, **24**, 599-606.

3 H.O.A Meyer, In *Mantle Xenoliths*; P.H. Nixon Ed.; John Wiley & Sons: Chichester, 1987; p.844.

4 D.G. Pearson, S.B. Shirey, In: *Application of Radiogenic Isotopes to Ore Deposit Research and Exploration.* Reviews in Economic Geology; D.D. Lambert, J. Ruiz Eds.; Society of Economic Geologists, Littleton CO: Denver, 1999, p.199.

5 J.W. Harris, J.J. Gurney, In *The properties of diamond*; J.E. Field Ed.; Academic Press: London, 1979, p. 674.

6 J.L. Orlov, *The mineralogy of diamond*; Wiley: New York, 1977.

7 N.V. Sobolev, *Deep-seated inclusions in kimberlites and the problem of the composition of theupper mantle*; American Geophysical Union: Washington, DC, 1977.

8 O. Leeder, R. Thomas, W. Klemm, *Einschlusse in Mineralien*; VEB Deutscher Verlag fur Grunstoffen industrie: Leipzig, 1987.

9 J.L.G. Fierro, *Metal Oxides-Chemistry and Applications*; Taylor and Francis: Boca Raton, FL, 2006.

10 J.R. Rostrup-Nielsen, *Catalysis-Science and Technology*; Springer-Verlag: Berlin, 1984, vol. 5, pp. 1–130.

11 S.D. Jackson, *Metal Oxide Catalysis*; Wiley-VCH Verlag GmbH & Co.: Weinheim, 2009, vol. 2, p. 485.

12 N.J. Van der Laag, C.M. Fang, G. de With, G.A. de Wijs, H.H. Brongersma, *J. Am. Ceram. Soc.*, 2005, **88**, 1544-1548.

13 C.M. Fang, S.C. Parker, G. de With, *J. Am. Ceram. Soc*., 2000, **83**, 2082-2084.

14 M.J. Davies, S.C. Parker, G.W. Watson, *J. Mater. Chem.*, 1994, **4**, 813-816.

15 F.F. Canova, A.S. Foster, M.K. Rasmussen, K. Meinander, F. Besenbacher, J.V. Lauritsen, *Nanotechnology*, 2012, **23**, 325703.

16 M.K. Rasmussen, A.S. Foster, B. Hinnemann, F.F. Canova, S. Helveg, K. Meinander, N.M. Martin, J. Knudsen, A. Vlad, E. Lundgren, A. Stierle, F. Besenbacher, J.V. Lauritsen, *Phys. Rev. Lett.*, 2011, **107**, 036102.

17 F.R. Massaro, M. Bruno, F. Nestola, *Crystal Growth & Design*, 2014, **14**, 2357-2365.

18 R. Smith, D. Bacorisen, B.P. Uberuaga, K.E. Sickafus, J.A. Ball, R.W. Grimes, *J. Phys.: Condens. Mater.*, 2005, **17**, 875-892.

19 A.D. Becke, *J. Chem. Phys.*, 1993, **98**, 5648-5652.

20 C. Lee, W. Yang, R.G. Parr, *Phys. Rev. B*, 1998, **37**, 785-789.

21 P.J. Stephens, F.J. Devlin, C.F. Chabalowski, M.J. Frisch, *J. Phys. Chem.*, 1994, **98**, 11623-11627.

22 M. Bruno, F.R. Massaro, M. Prencipe, R. Demichelis, M. De La Pierre, F. Nestola, *Journal of Physical Chemistry C*, 2014, **118**, 2498-2506.

23 J.D. Gale, *J. Chem. Soc. Faraday Trans.*, 1997, **93**, 629-637.

24 R. Dovesi, B. Civalleri, R. Orlando, C. Roetti, V.R. Saunders, In *Reviews in Computational Chemistry*; B.K. Lipkowitz, R. Larter, T.R. Cundari Eds.; John Wiley & Sons, Inc.: New York, 2005, vol.1, p.443.

25 R. Dovesi, B. Orlando, B. Civalleri, C. Roetti, V.R. Saunders, C.M. Zicovich-Wilson, *Z. Kristallogr*, 2005, **220**, 571-573.

26 R. Dovesi *et al.*, *CRYSTAL09 User's Manual*; University of Torino: Torino, Italy, 2009.

27 C. Pisani, R. Dovesi, C. Roetti, *Hartree-Fockab-initio treatment of crystalline systems*, Lecture Notes in Chemistry; Springer: Berlin, Heidelberg, New York, 1988.

28 Y. Noel, M. Catti, P. D'Arco, R. Dovesi, *Phys. Chem. Min.*, 2006, **33**, 383-393.

29 R. Demichelis, B. Civalleri, M. Ferrabone, R. Dovesi, *Int. J. Quantum Chem.*, 2010, **110**, 406-415.

30 M.F. Peintinger, D. Vilela Oliveira, T. Bredow, *J. Comput. Chem.*, 2013, **34**, 451-459.

31 M. Bruno, *Crystal Research & Technology*, 2013, **48**, 811-818.

32 M. Bruno, F.R. Massaro, M. Prencipe, D. Aquilano, *CrystEngComm*, 2010, **12**, 3626-3633.

33 M. Bruno, D. Aquilano, M. Prencipe, *Crystal Growth & Design*, 2009, **9**, 1912-1916.

34 M. Bruno, F.R. Massaro, M. Prencipe, *Surface Science*, 2008, **602**, 2774-2782.

35 M. Bruno, D. Aquilano, L. Pastero, M. Prencipe, *Crystal Growth & Design*, 2008, **8**, 2163-2170.

36 K. Reuter, M. Scheffler, *Phys. Rev. B*, 2001, **65**, 035406.

37 M. Rubbo, M. Bruno, M. Prencipe, *Crystal Growth & Design*, 2009, **9**, 404-408.

Figure captions

Figure 1. The spinel (100) reconstruction slice cells according to the *cut1* (left) and the *cut2* (right). The structure is viewed along the [100] direction. The colours stand: red for the O bonded to Mg (O1), purple for the O bonded only to Al (O2), greenish for the Al and blue for the Mg ions. The symmetry elements (the two-fold axes and the *m* planes) are reported as well.

Figure 2. The sixteen (100) cell configurations that preserve some of the initial symmetry elements after the reconstruction.

Figure 3. The spinel (110) reconstruction slice cells according to the *cut1* (left) and the *cut2* (right). The structure is viewed along the [110] direction.

Figure 4. The fifteen (110) surface configurations that preserve some of the initial symmetry elements after the reconstruction.

Figure 5. A comparison between the {100} surfaces of spinel realized according the *cut1* (up) and the *cut2* (down), and referring to the geometry optimization performed by empirical (on the left) and *ab initio* calculations according to the BS1 (in the middle) and the BS2 (on the right). The structures are projected along the equivalent <100> directions.

Figure 6. The {110} surfaces of spinel realized according the *cut1* (left) and the *cut2* (right). The geometries are optimized by empirical calculations. The structure is projected along the [110] direction.

Graphical abstract

A detailed configurational analysis of the {100} and {110} crystallographic forms of the spinel *sensu stricto* ($MgAl_2O_4$) has been performed.

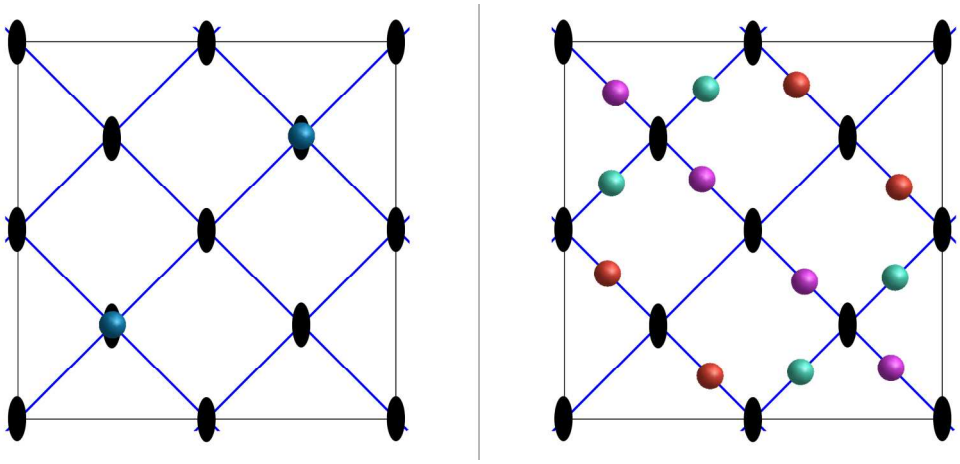

Fig.1

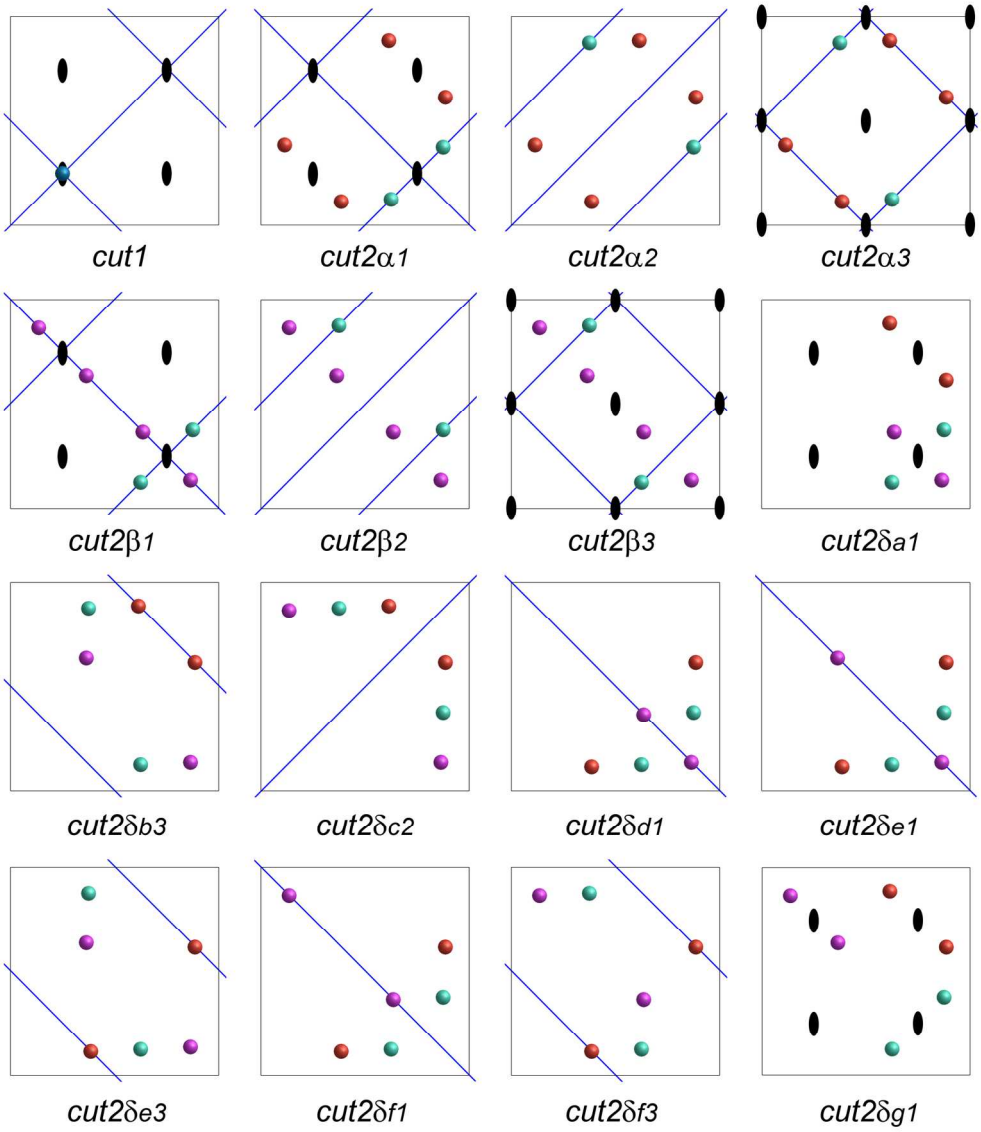
cut1
cut2α1
cut2α2
cut2α3
cut2β1
cut2β2
cut2β3
cut2δa1
cut2δb3
cut2δc2
cut2δd1
cut2δe1
cut2δe3
cut2δf1
cut2δf3
cut2δg1

Fig.2

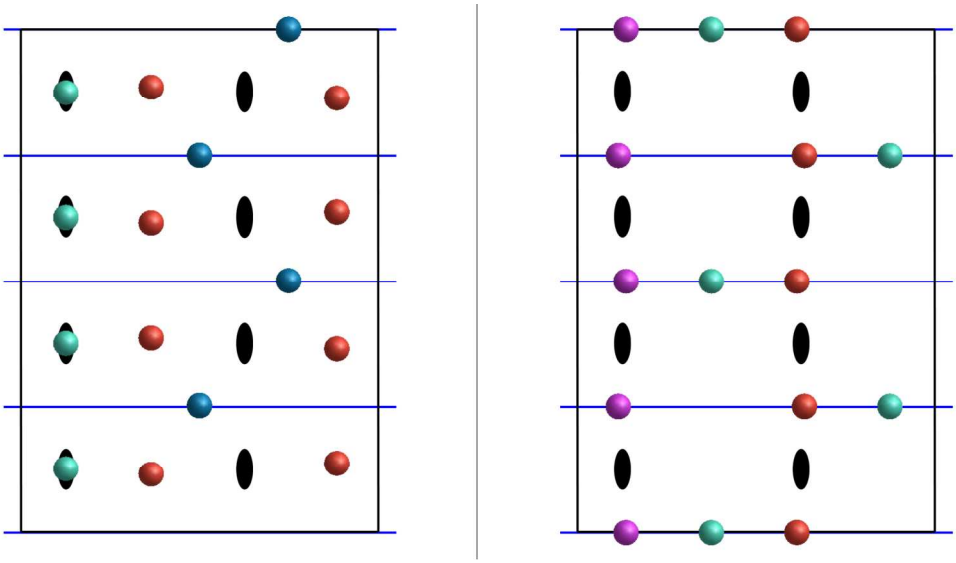

Fig.3

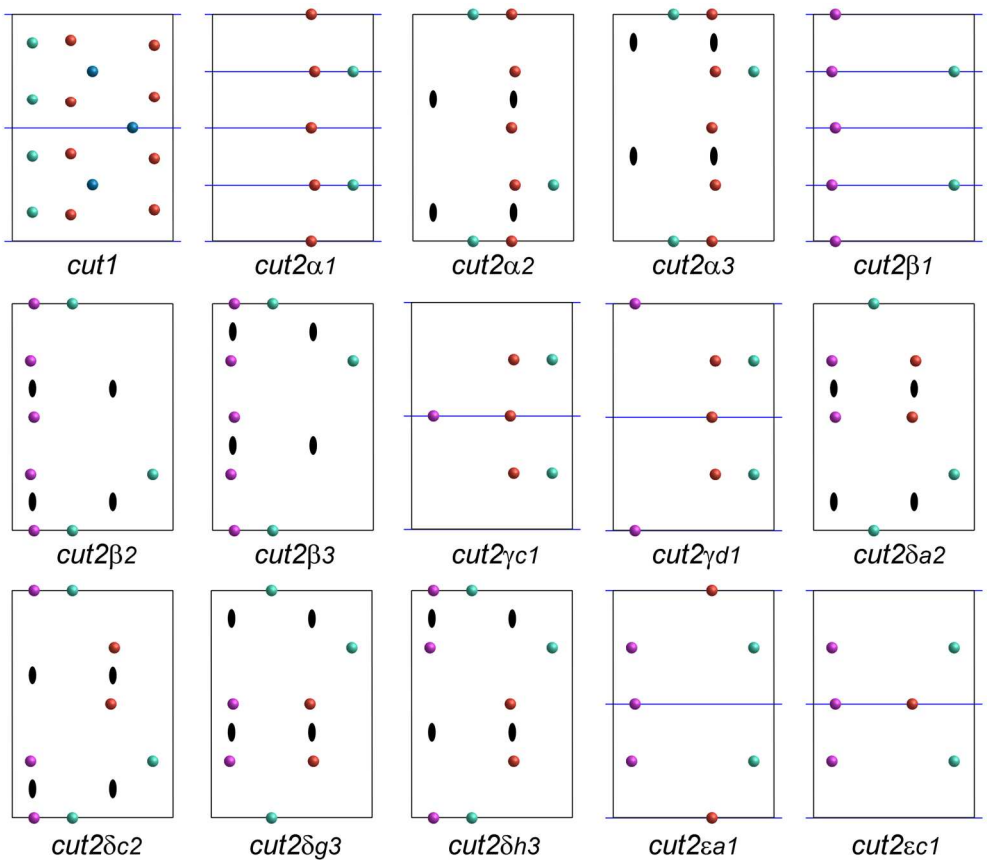
cut1
cut2α1
cut2α2
cut2α3
cut2β1
cut2β2
cut2β3
cut2γc1
cut2γd1
cut2δa2
cut2δc2
cut2δg3
cut2δh3
cut2εa1
cut2εc1

Fig. 4

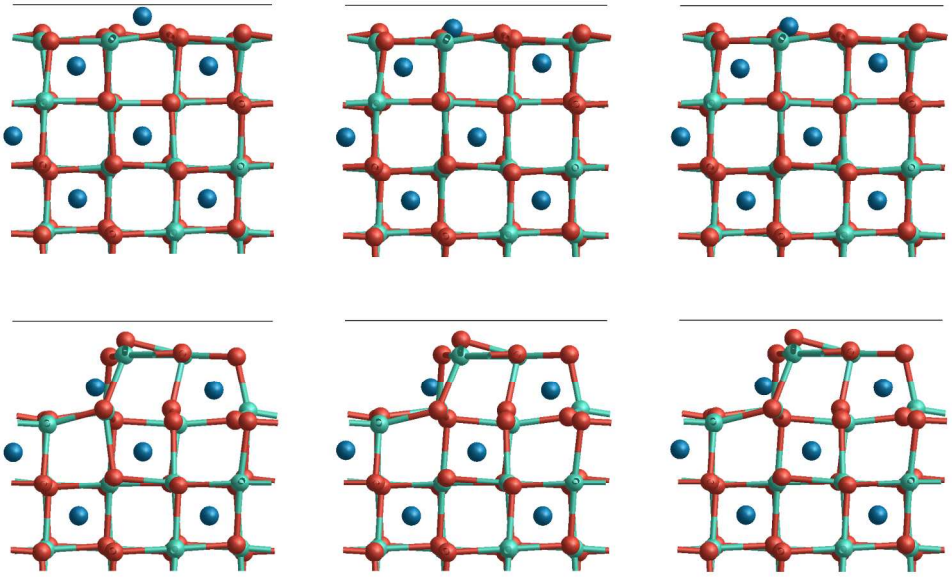

Fig. 5
203x122mm (300 x 300 DPI)

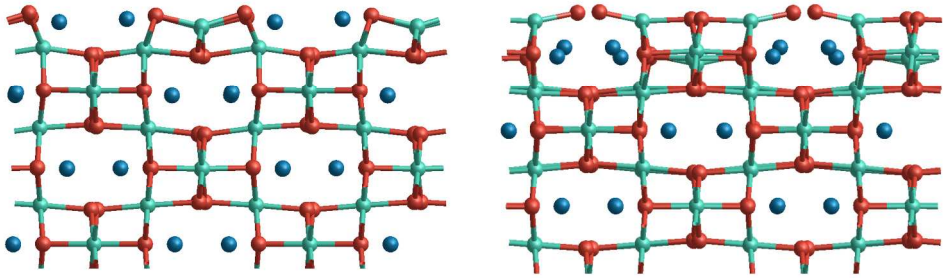

Fig. 6
169x50mm (300 x 300 DPI)